International Symposium
On Turbulence and Shear Flow
Phenomena (TSFP-9)
June 30 - July 3, 2015 *Melbourne, Australia*

POLLUTANT DISPERSION IN NEUTRAL AND STABLE BOUNDARY LAYERS ENTERING AN URBAN ENVIRONMENT

Jasper M. Tomas
Department Process & Energy, Lab. for Aero & Hydrodynamics, Delft University
Leeghwaterstraat 21, 2628 CA Delft, The Netherlands
j.m.tomas@tudelft.nl

Mathieu J.B.M. Pourquie
Department Process & Energy, Lab. for Aero & Hydrodynamics, Delft University
Leeghwaterstraat 21, 2628 CA Delft, The Netherlands
m.j.b.m.pourquie@tudelft.nl

Heerke E. Eisma
Department Process & Energy, Lab. for Aero & Hydrodynamics, Delft University
Leeghwaterstraat 21, 2628 CA Delft, The Netherlands
h.e.eisma@tudelft.nl

Harmen J.J. Jonker
Department Geoscience and Remote Sensing, Delft University
PO box 5048, 2600 GA Delft, The Netherlands
h.j.j.jonker@tudelft.nl

ABSTRACT

A smooth wall turbulent boundary layer (BL) approaching an array of cubes with dimensions $h \times h \times h$ has been studied with Large-Eddy Simulation (LES) to give insight in the development of the urban boundary layer (UBL). Pollutant dispersion in both neutral and stable conditions was considered. The surface forces reached a steady state after approximately $14h$ (= 7 streets). Up to that distance the vertical advective pollutant emission from the streets is significant compared to the turbulent pollutant emission. The stable case reached 1.85 times higher concentrations than the neutral case throughout the canopy, which shows stratifications effects cannot be neglected in urban environments.

INTRODUCTION

Because of the global trend of urbanization there is an increasing demand for accurate predictions of urban air quality levels. Therefore, predicting the dispersion behaviour of pollutants within the urban canopy is of great interest. The modelling and simulation of the UBL is usually done by assuming a BL that has fully developed over a large urban area with uniform properties (e.g. Michioka *et al.* (2013), Boppana *et al.* (2014)). However, in reality the overall character of the surface roughness changes from rural to suburban to urban, which means the BL has to adapt to the changing surface roughness. Moreover, often the UBL is considered only for (near-) neutral conditions by assuming that the turbulence added by the presence of the obstacle results in a well-mixed flow with nearly uniform temperature. In rural BLs pollutant concentrations increase significantly with increasing stability because the spreading downwind of the emission source is reduced due to lower turbulence levels. In urban environments stable BLs occur less often than unstable BLs (Wood *et al.* (2010)). However, because of potentially decreased air quality levels it is important to know when the 'neutral UBL assumption' is valid. The study presented here employs LES of a smooth wall turbulent BL exposed to a roughness transition consisting of an array of cubes in an in-line arrangement. A line source of pollutant emission is located in front of the array. The Reynolds number, $Re_\tau = u_\tau h/\nu$, based on the friction velocity u_τ at the inlet and the obstacle height h is 195. The case is studied for both neutral and stable conditions. The goal is to try to answer the following questions:

1. How does the rural boundary layer change into the urban boundary layer?
2. What is the influence of thermal stratification on this roughness transition?
3. How do the roughness transition and thermal stratification influence pollutant dispersion?

NUMERICAL METHOD

Governing Equations And Numerical Method

The filtered Navier-Stokes equations in the Boussinesq approximation are:

$$\frac{\partial \widetilde{u}_i}{\partial x_i} = 0, \tag{1}$$

$$\frac{\partial \widetilde{u}_i}{\partial t} = -\frac{\partial}{\partial x_j}\left(\widetilde{u}_i\widetilde{u}_j\right) - \frac{\partial}{\partial x_i}\left(\widetilde{p}/\rho_0 + \tau_{kk}/3\right) + \frac{g}{\theta_0}\widetilde{\theta}\delta_{i3} + \nu\frac{\partial^2 \widetilde{u}_i}{\partial x_j^2} + \frac{\partial}{\partial x_j}\left(2\nu_{sgs}S_{ij}\right), \tag{2}$$

$$\frac{\partial \widetilde{\varphi}}{\partial t} = -\frac{\partial}{\partial x_j}\left(\widetilde{\varphi}\widetilde{u}_j\right) + \frac{\nu}{Pr}\frac{\partial^2 \widetilde{\varphi}}{\partial x_j^2} + \frac{\partial}{\partial x_j}\left(\frac{\nu_{sgs}}{Pr_{sgs}}\frac{\partial \widetilde{\varphi}}{\partial x_j}\right) + \mathscr{S}, \tag{3}$$

where $\widetilde{(..)}$ denotes filtered quantities, $\widetilde{p}/\rho_0 + \tau_{kk}/3$ is the modified pressure, τ_{kk} is the trace of subgrid-scale stress

tensor, g is the gravitational acceleration, ν is the fluid's kinematic viscosity, ν_{sgs} is the subgrid-scale viscosity, Pr is the Prandtl number, Pr_{sgs} is the subgrid-scale Prandtl number, $S_{ij} = \frac{1}{2}\left(\frac{\partial \widetilde{u}_i}{\partial x_j} + \frac{\partial \widetilde{u}_j}{\partial x_i}\right)$ is the rate of strain tensor and $\mathscr{S}$ is a source term. Equation 3 describes the transport equation for all scalar quantities φ, which are the temperature θ and pollutant concentration c^*. From here on the $\widetilde{(..)}$ symbol will be omitted for clarity. Furthermore, the $\overline{(..)}$ symbol resembles time-averaging.

The code developed for this study is based on DALES (Heus *et al.* (2010)). The main modifications are the addition of an immersed boundary method (Pourquie *et al.* (2009)), the implementation of inflow/outflow boundary conditions and the application of the eddy-viscosity subgrid model of Vreman (2004). The equations of motion are solved using second-order central differencing for the spatial derivatives and an explicit third-order Runge-Kutta method for time integration. For the scalar concentration field the second-order central κ-scheme is used to ensure positivity. The simulations are wall-resolved, so no use is made of wall-functions. Pr was 0.71 and Pr_{sgs} was set to 0.9, equal to the turbulent Prandtl number found in the major part of the TBL in DNS studies by Jonker *et al.* (2013). The subgrid-scale Schmidt number was set to 0.9 as well. The code has been applied before to simulate turbulent flow over a surface-mounted fence, showing excellent agreement with experimental data (Tomas *et al.* (2015*a*), Tomas *et al.* (2015*b*)).

Simulation Set-up

Four types of simulations were performed:

Roughness Transition (RT) simulations: In these simulations the roughness transition is simulated by considering a smooth wall BL of height $10h$ that approaches an array of cubes with dimensions $h \times h \times h$ in an in-line arrangement equally spaced with a pitch of $2h$. A line source of pollutant is located at $2h$ in front of the first row of cubes. Both neutral and stable conditions are considered.

Driver (D) simulations: These were used to generate the smooth wall inflow BLs of $10h$ high for the RT simulations. Inflow and outflow conditions are used in the streamwise direction. The instantaneous inlet values are generated by the recycling method proposed by Lund *et al.* (1998) for the velocity and by a similar method by Kong *et al.* (2000) for the temperature. Both neutral and stable conditions are considered. The friction Reynolds number was 195.

Periodic Roughness (PR) simulation: This simulation uses the classical approach of applying periodic boundary conditions in the horizontal directions to simulate fully developed flow. The same roughness geometry as in the RT simulations is considered.

Validation (V) simulation: This simulation was done to compare with the experimental results from Castro *et al.* (2006) considering fully developed flow over an array of cubes. The geometry was similar to the RT and PR simulations except that the cube arrangement was staggered. As in the PR simulation periodic boundary conditions are used in the horizontal directions. The friction Reynolds number was 371.

Table 1 summarizes the domain size and number of grid points used in each type of simulation.

Boundary Conditions

In spanwise direction periodicity was assumed for all variables. On the ground and obstacle walls no slip conditions were applied, while at the top boundary a free slip condition was used. For the scalars θ and c^* zero-flux boundaries were assumed, except for θ at the ground and the top of the obstacles, for which isothermal conditions ($\theta = \theta_0$) were applied.

Table 1. Domain dimensions and grid sizes.

Sim.	L_x	L_y	L_z	N_x	N_y	N_z
RT	$61.47h$	$18h$	$30h$	1080	360	180
D	$200h$	$18h$	$30h$	768	320	128
PR	$8h$	$8h$	$20h$	160	160	144
V	$4h$	$4h$	$10h$	64	80	112

Driver (D) and Roughness Transition (RT) Simulations. Velocity and temperature data were imposed at the inlet as described in the previous section. This inflow satisfied a constant mass flux. At the outlet a convective outflow boundary condition was applied for all variables. At the top boundary a constant outflow velocity of $w = U_\infty \overline{d\delta_1/dx}$ was used, where $\overline{d\delta_1/dx}$ is the mean streamwise growth of the displacement thickness. This was done to establish a zero-pressure gradient in the driver simulations. The RT simulations used the same outflow velocity as the D simulations.

Periodic Roughness (PR) and Validation (V) Simulations. Periodicity was assumed in the horizontal directions and the flow was driven by a constant streamwise pressure gradient, $\partial\Pi/\partial x = u_\tau^2/L_z$, with $\Pi = \widetilde{p}/\rho_0 + \tau_{kk}/3$.

RESULTS

Statistics

In all simulations statistics were computed after a steady state was reached. This was after 10.000 time scales, $T = h/U_\infty$. The driver simulations required $20.000T$, starting from a coarse mesh simulation. The RT simuations ran for $1300T$ of which the last $800T$ were used for computing statistics using an interval of $0.2T$. A constant time step of $0.01T$ was used in the neutral simulations and $0.02T$ in the stable simulation.

Validation (V) simulation

The V simulation was done to validate the model with experimental data from Castro *et al.* (2006). Figure 1 shows the vertical profile of mean streamwise velocity at four locations indicated in the schematic in the figure. The agreement is quite satisfactory. However, the simulation overpredicts the length of the wake of the upstream cube, which causes a difference with the experimental data at location P3. Figure 2 shows the mean resolved Reynolds stress, $\overline{u'w'}$, at locations P1 and P2. Unfortunately, experimental data is not available at location P3. The agreement between the model and experimental results is good, although the vertical resolution was too low to resolve the peak caused by the shear layer emanating from the top of the cube. This probably also affected the aforementioned wake length. The ver-

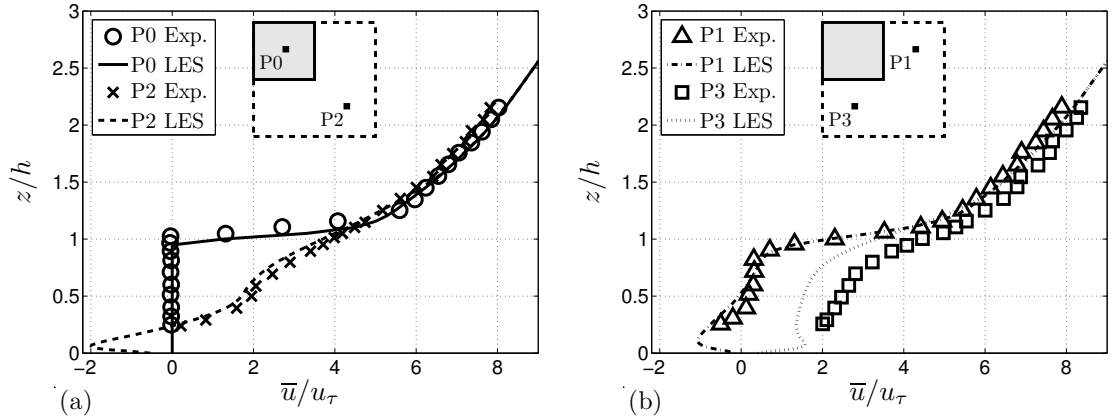

Figure 1. Mean streamwise velocity at stations P0 and P2 (a) and P1 and P3 (b). Experimental data from Castro *et al.* (2006).

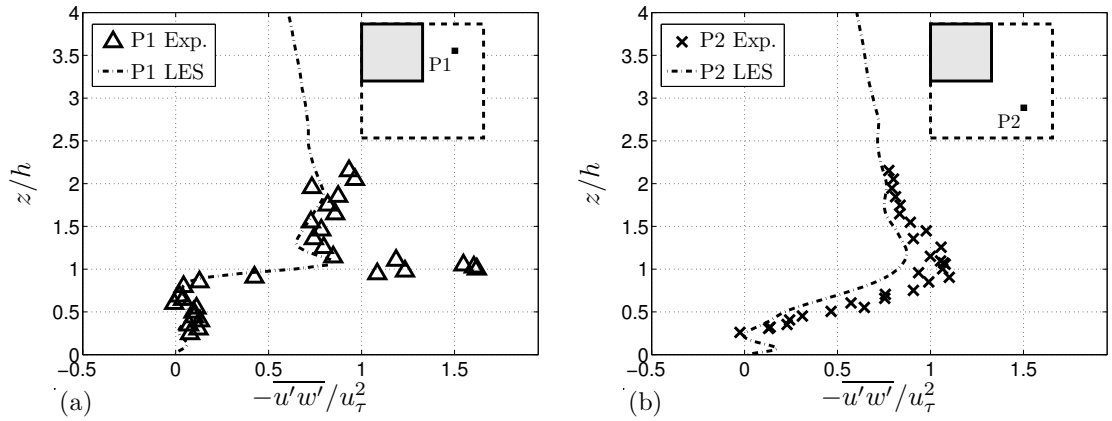

Figure 2. Mean Reynolds stress at stations P1 and P2. Experimental data from Castro *et al.* (2006).

tical cell size at the top of the cubes was $1/20h$. In the RT and PR simulations this was decreased to $1/100h$ in order to capture the shear layer.

Driver (D) and Roughness Transition (RT) simulations

Two RT simulations were done; one for neutral conditions and one for stable conditions. Two corresponding D simulations were done to generate the inflow. In the stable case the bulk Richardson number

$$Ri = \frac{(g/\theta_0)(\theta_\infty - \theta_0)\,\delta}{U_\infty^2}, \tag{4}$$

was 0.147. In the D simulation the resulting gradient Richardson number

$$Ri_{grad} = \frac{g}{\theta_0}\frac{\partial\overline{\theta}}{\partial z}\Big/ 2S_{ij}S_{ij}\,, \tag{5}$$

was 0.2 throughout most of the BL. Increasing the stratification even more resulted in intermittent turbulence. Figure 6 (last page) shows the contours of instantaneous velocity magnitude normalized with U_∞ for the neutral (top) and the stable (bottom) case. At the inlet the flow is already turbulent (generated in the D simulations). Low speed streaks are visible in the horizontal plane at $z = 0.1h$. In the midplane both the neutral and the stable case show small scale turbulence generated by the roughness elements. However, in the stable case the exchange of momentum in the outer region is reduced as can be seen by the more layered velocity contours.

Mean flow. The mean flow is statistically homogeneous in the spanwise direction only, because the flow is developing in the streamwise direction. Therefore, the mean flow is averaged in the spanwise direction and over a single pitch (i.e. a 'street') of $2h$ in the streamwise direction, indicated by $\langle..\rangle$. Figure 3 shows the spatially averaged mean forces for the neutral and the stable cases. The results of the PR simulation are also shown. The friction velocity u_τ is calculated from the total drag built up from skin frictional drag, $\frac{1}{2}C_f$, and form drag, P_d. When u_τ reaches a constant value this is an indication of fully developed flow at the obstacle height. At the inlet u_τ is $0.0374U_\infty$ for the neutral case and $0.0383U_\infty$ for the stable case. In the canopy the neutral case converges to a friction velocity 1.9 times larger than at the inlet. The stable flow experiences a lower drag increase by the canopy because at the end of the domain the friction velocity is 1.6 times the inlet value. The drag due to skin frictional forces and due to pressure forces are shown as well (Figure 3b and 3c, respectively). At this Reynolds number form drag constitutes 81% (neutral) and

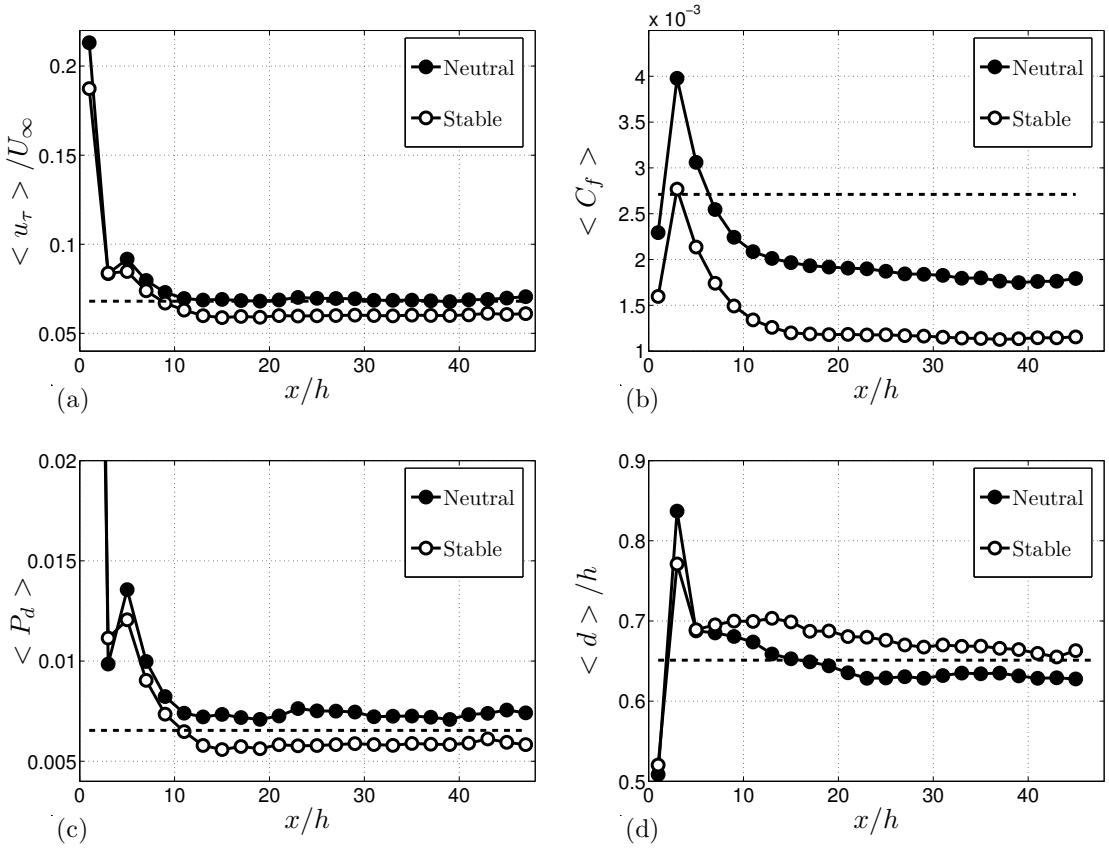

Figure 3. Mean street-averaged forces. (a) Friction velocity u_τ, (b) Skin friction coeffient C_f, (c) Form drag coefficient P_d, (d) Displacement height d. The dashed line corresponds to the PR simulation results.

84% (stable) of the total drag. This was 71% in the PR simulation because that simulation was done at a lower friction Reynolds number (based on the inlet friction velocity of the RT simulations). Finally, Figure 3d shows the displacement height for the three cases. The displacement height is the height at which the total drag force acts (Jackson (1981)). It is computed by dividing the total moment by the total drag force.

Pollutant dispersion. Figure 4 shows the contours of mean concentration at the midplane of the domain for both cases. The average concentration within the volume of each street, Φ, is in the stable case approximately 1.85 times larger than in the neutral case throughout the domain. The emission of pollutant out of the street can occur through the top of the canopy (E_{top}) and along the streets in streamwise direction (E_{str}):

$$E_{top} = \int_0^{2h}\int_0^{L_y} \frac{\langle \overline{wc}\rangle|_{z=h}}{U_\infty} dy\,dx \qquad (6)$$

$$E_{str} = \int_0^{h}\int_0^{L_y} \frac{\langle \overline{uc}\rangle|_{x=2h}}{U_\infty} dy\,dz, \qquad (7)$$

where the velocity is normalized by U_∞ and the concentration c^* is normalized by U_∞, the cube height h, the domain width L_y and the total emission Q: $c = c^* U_\infty h L_y / Q$. Figure 5a shows E_{top}/Φ at each street in terms of the advective ($= \overline{w}\,\overline{c}$) and turbulent ($= \overline{w'c'}$) contributions. The vertical subgrid flux constitutes $< 1\%$ of the total emission for the first $10h$. As the total flux decreases this becomes 20% (neutral) and 10% (stable) of the total flux at the end of the domain. Simulations on the same geometry using periodic boundary conditions by Michioka *et al.* (2013) showed that the turbulent flux at the top of the canopy is responsible for nearly 100% of the total flux. However, the results presented here show that the vertical advective flux is significant in the first 7 streets ($= 14h$) after which turbulence is the only significant contributor. For the horizontal flux (Figure 5b) advection is the only significant source throughout the canopy. After approximately 7 streets the advective part of E_{str}/Φ becomes constant, because $\overline{u}|_{z=h}$ approaches a constant value.

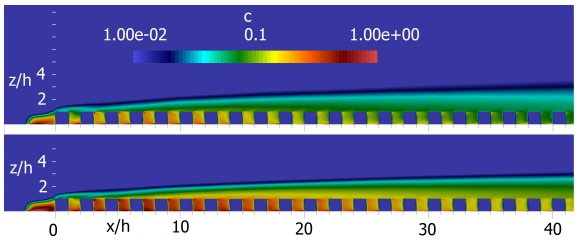

Figure 4. Contours of mean concentration in the x-z midplane. (Logarithmic scale). A spanwise line source is located $2h$ in front of the array at $z = 0.2h$. Top; neutral conditions. Bottom: stable conditions.

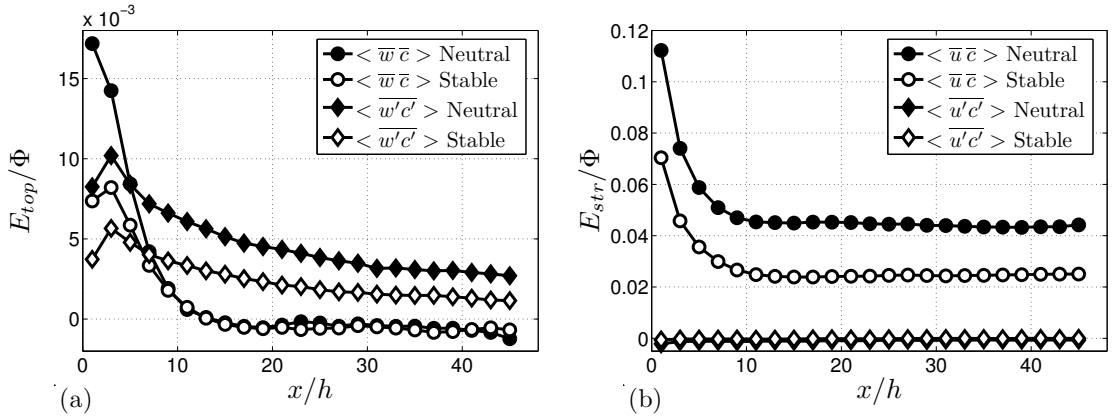

Figure 5. Mean pollutant emission from each street divided by mean concentration in that street. (a) Emission through top of canopy, E_{top}, (b) Horizontal emission through street, E_{str}. Advective and turbulent contribution to the total flux are shown. Subgrid fluxes are added to turbulent contribution.

CONCLUSIONS

A comparison of results from simulation V and experimental data shows that the model predicts the mean streamwise velocity and the mean Reynolds stress to a good approximation. In the subsequent RT and PR simulations the vertical grid resolution as well as the streamwise resolution were increased to accurately capture the shear layer at the height of the cubes. The RT simulations show that for both the neutral and the stable case the surface forces becomes constant after approximately 7 streets. The stable BL experiences a lower drag increase by the canopy than the neutral BL. In the canopy the mean concentration is approximately 1.85 times higher than for neutral conditions, which shows that stratification effects cannot be neglected in urban environments. Nevertheless, qualitatively the streamwise development of the emissions from each street are similar to the neutral case. In both cases the roughness transition causes a significant advective flux of pollutant. Future work will focus on the outer flow development, its interaction with the canopy flow and the influence of the roughness lay-out on dispersion.

ACKNOWLEDGMENTS

This study was done within the STW project DisTUrbE (project no. 11989) using the computational resources of SURFsara with the funding of the Netherlands Organization for Scientific Research (NWO).

REFERENCES

Boppana, V. B. L., Xie, Z.-T. & Castro, I. P. 2014 Thermal Stratification Effects on Flow Over a Generic Urban Canopy. *Boundary-Layer Meteorology* **153** (1), 141–162.

Castro, Ian P., Cheng, Hong & Reynolds, Ryan 2006 Turbulence Over Urban-type Roughness: Deductions from Wind-tunnel Measurements. *Boundary-Layer Meteorology* **118** (1), 109–131.

Heus, T., van Heerwaarden, C. C., Jonker, H. J. J., Pier Siebesma, A., Axelsen, S., van den Dries, K., Geoffroy, O., Moene, A. F., Pino, D., de Roode, S. R. & Vilà-Guerau de Arellano, J. 2010 Formulation of the Dutch Atmospheric Large-Eddy Simulation (DALES) and overview of its applications. *Geoscientific Model Development* **3** (2), 415–444.

Jackson, P. S. 1981 On the displacement height in the logarithmic velocity profile. *Journal of Fluid Mechanics* **111**, 15.

Jonker, Harm J. J., van Reeuwijk, Maarten, Sullivan, Peter P. & Patton, Edward G. 2013 On the scaling of shear-driven entrainment: a DNS study. *Journal of Fluid Mechanics* **732**, 150–165.

Kong, Hojin, Choi, Haecheon & Lee, Joon Sik 2000 Direct numerical simulation of turbulent thermal boundary layers. *Physics of Fluids* **12** (10), 2555–2568.

Lund, TS, Wu, Xiaohua & Squires, KD 1998 Generation of turbulent inflow data for spatially-developing boundary layer simulations. *Journal of Computational Physics* **140** (2), 233–258.

Michioka, Takenobu, Takimoto, Hiroshi & Sato, Ayumu 2013 Large-Eddy Simulation of Pollutant Removal from a Three-Dimensional Street Canyon. *Boundary-Layer Meteorology* **150** (2), 259–275.

Pourquie, M., Breugem, W. P. & Boersma, B. J. 2009 Some Issues Related to the Use of Immersed Boundary Methods to Represent Square Obstacles. *International Journal for Multiscale Computational Engineering* **7** (6), 509–522.

Tomas, J.M., Pourquie, M.J.B.M., Eisma, H.E., Elsinga, G.E., Jonker, H.J.J. & Westerweel, J. 2015*a* Pollutant dispersion in the urban boundary layer. In *Direct and Large-Eddy Simulation IX, ERCOFTAC Series Volume 20* (ed. Jochen Fröhlich, Hans Kuerten, Bernard J. Geurts & Vincenzo Armenio), pp. 435–441. Springer.

Tomas, J M, Pourquie, M.J.B.M. & Jonker, H J J 2015*b* The influence of an obstacle on flow and pollutant dispersion in neutral and stable boundary layers. *Atmospheric Environment* **113**, 236–246.

Vreman, A.W. 2004 An eddy-viscosity subgrid-scale model for turbulent shear flow: Algebraic theory and applications. *Physics of Fluids* **16** (10), 3670.

Wood, C. R., Lacser, a., Barlow, J. F., Padhra, a., Belcher, S. E., Nemitz, E., Helfter, C., Famulari, D. & Grimmond, C. S. B. 2010 Turbulent Flow at 190m Height Above London During 20062008: A Climatology and the Applicability of Similarity Theory. *Boundary-Layer Meteorology* **137** (1), 77–96.

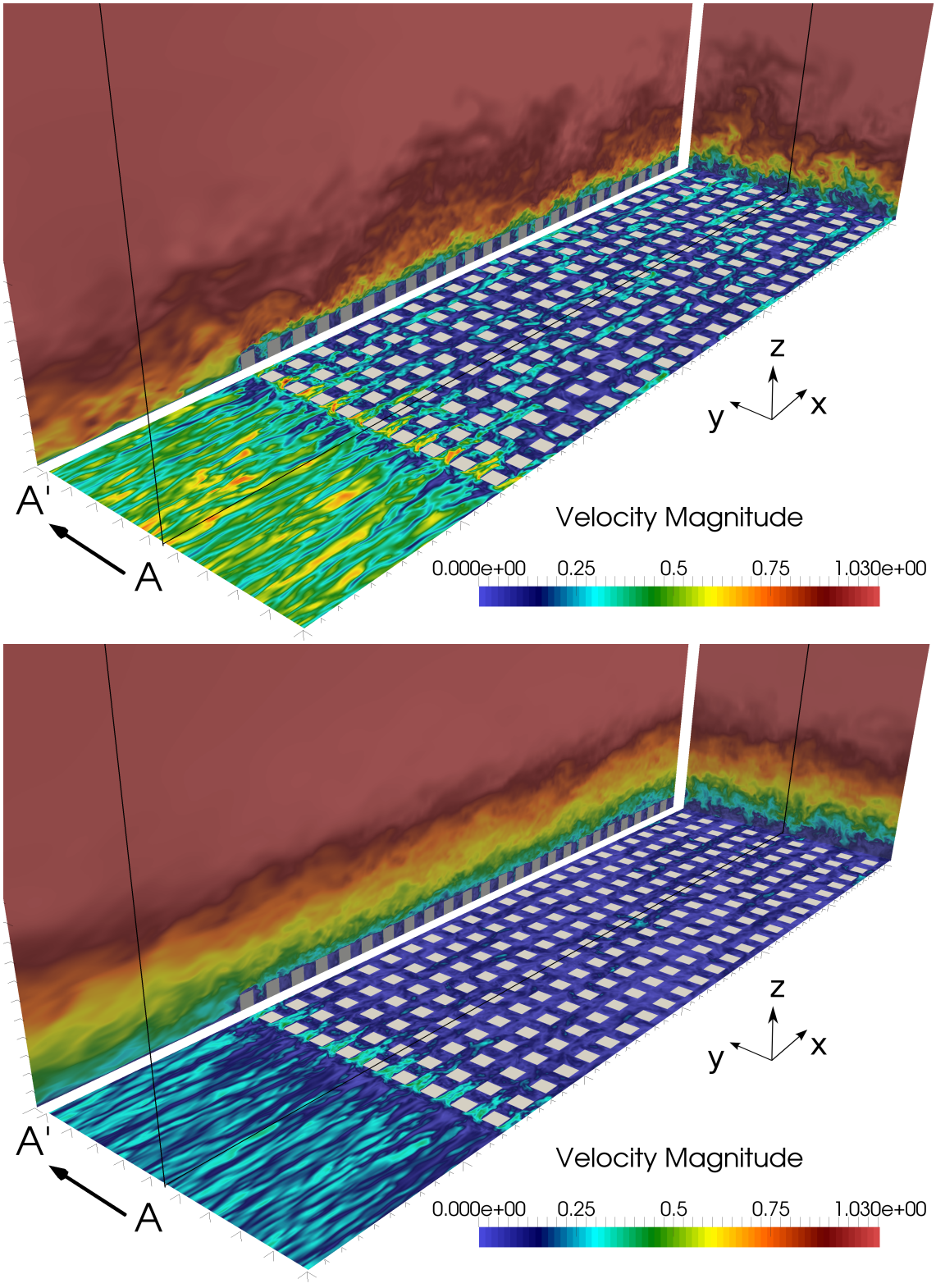

Figure 6. Instantaneous velocity magnitude contours for RT simulations; neutral (top) and stable stratification (bottom). Velocity magnitude is normalized with U_∞. Plane **A'** is a projection of midplane **A**. The x-y plane is located at $z/h = 0.1$ and cuts through the cubes.